Journal of Zhejiang University-SCIENCE A (Applied Physics & Engineering) in press
www.jzus.zju.edu.cn; www.springer.com/journal/11582
E-mail: jzus_a@zju.edu.cn

Research Article

https://doi.org/10.1631/jzus.A2400068

Impact of disc-cutter partial wear on tunneling parameters and a high-accuracy method for discrimination of partial wear

Xinghai ZHOU, Yakun ZHANG✉, Guofang GONG, Huayong YANG

State Key Laboratory of Fluid Power & Mechatronic Systems, Zhejiang University, Hangzhou 310058, China

Abstract: In tunnel construction with tunnel boring machines (TBMs), accurate knowledge of disc-cutter failure states is crucial to ensuring efficient operation and preventing delays and cost overruns. This study investigates the influence of disc-cutter partial wear on tunneling parameters and proposes a novel method for discriminating partial-wear ratio based on a stacking ensemble model. The time-domain features, including the mean and standard deviation, of torque and thrust are analyzed through a series of scaled-down experimental tests on partial wear. Torque and thrust values increase when a disc cutter becomes trapped and partially worn. The impact of the partial-wear ratio on tunneling parameters appears to be more significant than partial-wear depth. A total of 40 features are selected from the time domain, frequency domain, and time-frequency domain to describe the torque and thrust. The relationships between these features and the partial-wear ratio are analyzed using Pearson coefficients and Copula Entropy. The results reveal that, except for the form factor in the time-domain features, the remaining features exhibit certain linear or non-linear correlations with the partial-wear ratio. Lastly, the proposed model successfully achieves discrimination of the partial-wear ratio and outperforms other commonly used models in terms of overall classification accuracy and differentiation capability in different categories. This research provides effective support for monitoring and health management of disc-cutter failure states.

Key words: Tunnel boring machine (TBM); Disc cutter; Partial wear; Tunneling parameters; Multi-domain features; Ensemble learning

1 Introduction

Disc cutters are critical components of tunnel boring machines (TBMs) and play a vital role in the success of tunneling operations (Farrokh and Rostami, 2008; Bilgin and Algan, 2012). Despite being designed for harsh and unpredictable underground conditions (Zhang and Xiao, 2018a), disc cutters often experience high failure rates due to the high stresses and abrasion they encounter during operation (Acaroglu et al., 2008; Zhang and Xiao, 2018b; Yu et al., 2020). If a failed disc cutter is not replaced in time, it can lead to the failure of adjacent disc cutters and even damage to the cutterhead. Because of these high failure rates and the severe consequences, it is crucial to gather information about the health status of cutters and replace damaged ones in a timely manner (Yu et al., 2021). However, the current maintenance strategy for disc cutters still relies on periodic manual inspection (Hassanpour et al., 2014). This method requires shutting down a TBM and sending maintenance personnel into the TBM cutterhead. Not only does this pose significant safety risks, reduce TBM utilization, and increase construction costs (Wang et al., 2019), but it is also highly inefficient. Regular maintenance often results in either insufficient or excessive replacement of disc cutters. Statistics reveal that cutter consumption accounts for one-third of the total cost of tunnel construction, and the time spent on cutter inspection and replacement amounts to approximately one-third of the total project time (Li et al., 2018; Lan et al., 2019). To address this problem, the development of disc-cutter failure

✉ Yakun ZHANG, yakunzhang@zju.edu.cn
Xinghai ZHOU, https://orcid.org/0000-0002-3148-607X
Yakun ZHANG, https://orcid.org/0000-0002-1667-8700

Received Feb. 1, 2024; Revision accepted May 21, 2024;
Crosschecked

© Zhejiang University Press 2024

Unedited

detection and early warning technology has received significant research attention.

The state-of-the-art of disc-cutter fault-detection methods can be broadly classified into two categories: sensor-based real-time monitoring and data-driven prediction. The harsh operating conditions and limited installation space pose significant challenges to the development and application of sensor-based technologies. Additionally, the high cost of sensors and difficulties in signal transmission make it challenging to implement these technologies in actual construction sites, limiting their usage to laboratory environments (Liu et al., 2017). Data-driven approaches, on the other hand, aim to predict disc-cutter status via the excavation data (Li and Su, 2010; Yang and Qiu, 2016; Amoun et al., 2017). For instance, Hassanpour (Hassanpour, 2018) developed a relationship between cutter life and two main rock parameters including average mineral hardness and intact rock uniaxial compressive strength (UCS), and presented an empirical model for predicting average cutter life using the measured parameters of UCS and the Vickers hardness number of rock. Karami et al. (Karami et al., 2021) estimated the cumulative volumetric mass loss of disc cutters based on compressive strength index and rock-quality designation, and provided a chart to determine the wear on the disc cutters. These data-driven models, which are built by means of statistical analysis of large datasets, indicate that excavation parameters contain valuable information regarding the interaction mechanisms between worn disc cutters and rocks, enabling effective wear prediction. However, these studies primarily focus on normal wear, and there is a serious lack of research on abnormal damage, which is quite common in practice.

Unlike the gradual material removal observed in normal wear (Lin et al., 2020; Pan et al., 2020), abnormal damage occurs in various forms, such as partial wear, fracture, and edge curling (Zhang et al., 2017; Ren et al., 2018). Partial wear is the most common type of abnormal damage (Huang, 2021). Taking the tunneling project in Gaoligong Mountain in China as an example, partially worn cutters accounted for 58.3% of the total number of abnormally damaged cutters and 18.2% of the total worn cutters (Zhang, 2021), as illustrated in Fig. 1. Fig. 2 depicts the partial-wear state of the cutterhead from a decommissioned TBM. The consequences of such damage are significantly more severe compared to normal wear (Su et al., 2020). During the partial-wear process, the cutter ring quickly and partially wears due to cutter-bearing failure or foreign objects obstructing rotation around the cutter shaft, resulting in only a portion of the cutter making contact with the rock (Ko and Lee, 2020). The transition from a rolling to a sliding motion between the cutter ring and the rock surface intensifies wear at the contact point, accelerating the wear rate of adjacent disc cutters and leading to premature failure (Sun et al., 2023). If partially worn cutters are not replaced promptly, it can eventually jeopardize the entire cutter head and drive system. This poses significant safety risks and can result in substantial economic loss.

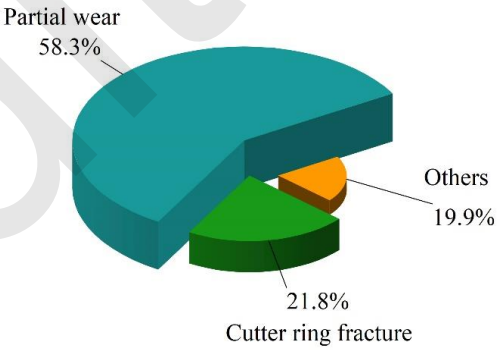

Fig. 1 Proportion of partially worn cutters out of total damaged cutters

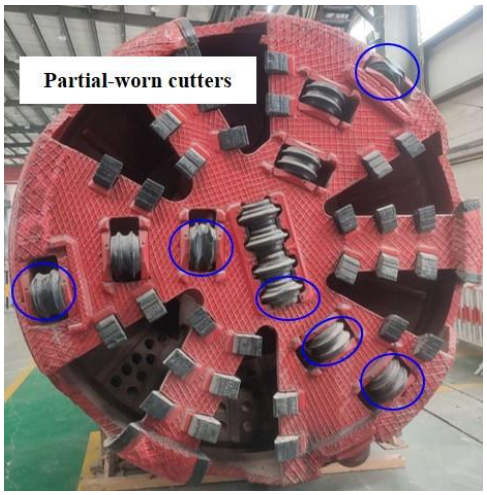

Fig. 2 Partially worn cutters in cutterhead

To assess the impact of partial wear, Sun et al. conducted rock-cutting experiments and analyzed changes in cutting force, rock fragmentation, and energy consumption (Sun et al., 2022; Sun et al., 2023). However, this research looked only at individual disc cutters, neglecting the influence of the quantity and extent of partial wear on the overall loading of the TBM. There is a notable deficiency in systematic research on partial wear. Knowledge gaps persist regarding alterations in tunneling parameters following partial wear, real-time and efficient detection of partial-wear occurrence, and evaluation of the degree of partial wear.

In order to fill these gaps, we investigated the differences in tunneling parameters between partially worn and normal disc cutters and developed models to evaluate partial-wear ratio, which will aid in construction operations and maintenance.

The remainder of this paper is organized as follows: we describe a series of experiments we carried out on both normal and partially worn cutters, based on a reduced-scale shield-test rig. Next, the acquisition and analysis of tunneling parameters, specifically torque and thrust, under different failure modes are covered. Finally, a high-performance discrimination method of partial-wear ratio (based on ensemble learning) is proposed and our efforts to verify it are outlined, leading to some conclusions.

2 Experiment and Analysis

The experimental setup and procedure for investigating partial wear of disc cutters are described in this section. Accurate and reliable excavation parameters were obtained through a meticulously designed experimental setup that was capable of reproducing the excavation process. The procedure was a systematic approach to conducting the experiments and capturing the wear patterns observed in the disc cutters. Additionally, we performed comprehensive analysis to further interpret the experimental results.

2.1 Experimental Setup

The tunneling process of a TBM involves numerous operational parameters that are challenging to scale down entirely. This study focused on experiments related to partial wear, with a reduced-scale shield-test rig. Key parameters under investigation included cutterhead and disc-cutter size and material, thrust force, advance speed, cutterhead rotation speed, and cutterhead torque. The technical specifications of the test rig and the TBM used at the Zhengzhou Metro construction site adhered to the following scaling criteria: (1) The materials of the cutterhead and disc cutter on the test rig matched those of the actual TBM. The actual TBM had a diameter of 6000mm, while the test rig measured 350mm, resulting in a geometric scale ratio of 17:1. Additionally, the actual disc cutter had a diameter of 483mm, whereas the test disc cutter measured 48.3mm, resulting in a geometric scale ratio of 10:1. (2) Test-rig thrust force was proportional to the TBM's actual thrust force. (3) Test-rig advance speed aligned with the TBM's actual advance speed. (4) Cutterhead torque in the test rig was proportional to the TBM's actual cutterhead torque. (5) Cutterhead rotation speed in the test rig matched the actual rotation speed of the TBM.

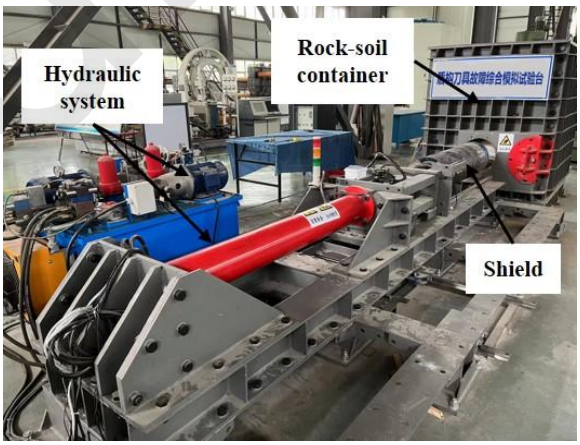

Fig. 3 The reduced-scale shield-test rig for experiments on partial wear

Fig. 3 illustrates the test rig, consisting of a hydraulic system, shield and rock-soil container. Table 1 details the main technical specifications of the test rig. The horizontal movement of the shield was controlled by the hydraulic system, while the rotation was driven by a servo motor. The cutterhead was installed at the front of the shield machine, and the normal and partially worn disc cutters were arranged on it using bolts.

Unedited

Table 1 Main technical specifications of the test rig

Technical parameter	Design value
Overall dimensions (mm)	4300×866×1300
Cutterhead diameter (mm)	350
Disc-cutter diameter (mm)	48.3
Maximum stroke (mm)	1300
Cutterhead Rotation Speed (r/min)	0-10
Maximum allowable torque (N·m)	1000
Advancing speed (mm/min)	0-50
Size of rock-soil container (mm)	1200×1500×1500

The compound cutterhead was specifically designed to primarily drive the rotation of the disc cutters for rock-breaking, as depicted in Fig. 4a. It can be seen that there are 15 cutter seats distributed on the cutterhead, of which 12 are equipped with 12 face disc cutters, evenly distributed at an angle of 60 degrees; and that the outer circle has 3 seats equipped with 3 edge disc cutters, distributed at an angle of 120 degrees and tilted at an angle of 10 degrees. For convenience of description, the 15 disc cutters are numbered and their installation radii are shown in Fig. 4a and Table 2. Numbers 1 to 12 are face disc cutters, and numbers 13 to 15 are edge disc cutters. The scrapers are also divided into three groups at an angle of 120 degrees, with 8 in each group, and installed on the opening edge of the cutterhead. The dimensions of the scrapers were scaled down to a ratio of 1:10, following the general practice in engineering.

(a) ①-cutter seat; ②-disc cutter; ③-scraper

(b)

Fig. 4 Cutterhead: (a) schematic structure and disc-cutter numbering diagram, (b) Assembly of the cutterhead

In engineering applications, partial wear of disc cutters is typically caused by bearing failure or obstructions preventing rotation around the cutter shaft, causing a relative motion transition from rolling to pure sliding between the cutter and the rock (Zhang, 2011). To faithfully recreate the substantial disparities between normal and partially worn cutters, we used effective structural designs for the experimental cutter seat and disc cutter. Fig. 5 illustrates that the cylindrical ends of the normal cutter were replaced with a square structure and the cutter seat was modified as well, which enabled the cutter to be jammed during the shield tunneling process, resulting in a "trapped cutter". In this case, the cutter ring did not undergo any wear. When the outer contour of the cutter no longer exhibits a complete circular shape, it is referred to as a partially worn cutter (see Fig. 6). The geometric profile of the contact area can be divided into two regions: the arc surface and the plane. The depth of partial wear is defined as the difference between the radius and the perpendicular distance from the disc cutter's center to the contact plane. To simulate this scenario accurately, the designed cutters were subjected to linear cuts, creating a flat surface on one side, mimicking the effect of partial wear. Various depths of partial wear were then simulated by successively removing 0.5mm, 1.0mm, 1.5mm, and 2.0mm from the cutting ring. The corresponding real partial-wear depths are 5mm, 10mm, 15mm, and 20mm.

Table 2 Installation radius of disc cutters

Number	Installation radius (mm)	Number	Installation radius (mm)
1	65	2	70
3	75	4	80
5	85	6	90
7	120	8	125
9	130	10	135
11	140	12	145
13	147	14	149
15	151		

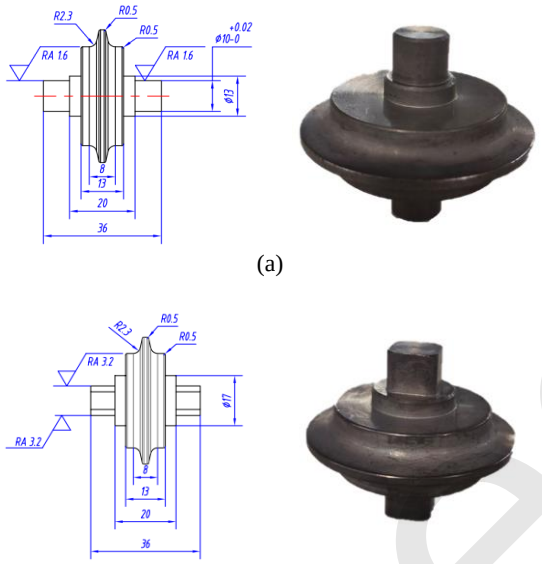

(a)

(b)

Fig. 5 Structural design of disc cutters: (a) Normal cutter, (b) Trapped cutter

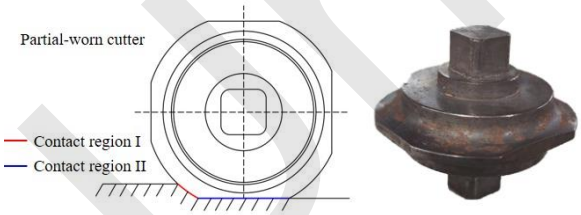

Fig. 6 Partially worn cutter

Table 3 Properties of the experimental materials

Properties	Soft soil	Sandstone
Moisture Content (%)	9.86	6.6
Porosity	60.4	6.6
Compressibility	0.57	0.64
Internal Friction Angle (□)	26	27.2
Cohesive Strength (KPa)	26	28
Shear Modulus (KPa)	15	18

A composite strata consisting of soft soil on top and sandstone on the bottom was selected for shield tunneling and placed in the rock-soil container. All the materials used in the experiments were collected from the same construction site of the Zhengzhou Metro to ensure consistency of composition and strength. The rock-soil properties are presented in Table 3. The dimensions of the rock-soil container were 1200×1500×1500, significantly larger than the excavation diameter of the shield, thereby eliminating the influence of limited boundaries in the experiments. To enable real-time excavation-data collection, we implemented a comprehensive data-acquisition and monitoring system. This system recorded various parameters, including cutterhead speed, advance speed, and cutterhead torque and thrust, at a sampling frequency of 1 Hz. High-precision torque sensors (0-1000 Nm) and wheel-type pressure sensors (0-80 tons) were used to measure the cutterhead torque and thrust, respectively. The cutterhead speed and advance speed were obtained from the signal output ports of a servo motor driver.

2.2 Experimental Procedure

The experimental procedure is detailed in the Electronic Supplementary Materials.

Table 4 Disc-cutter parameters of the test groups

Index	Proportion	Numbers	Types of cutters	Partial-wear depth (mm)
1#	0	/	Normal	0
2#	25%	10,11,12	Trapped	0
3#-1			Partial-worn	0.5
3#-2				1.0
3#-3				1.5
3#-4				2.0
4#	50%	7,8,9, 10,11,12	Trapped	0
5#-1			Partial-worn	0.5
5#-2				1.0
5#-3				1.5
5#-4				2.0
6#	75%	4,5,6, 7,8,9, 10,11,12	Trapped	0
7#-1			Partial-worn	0.5
7#-2				1.0
7#-3				1.5
7#-4				2.0

Uncorrected

In order to investigate the impact of partial wear on excavation parameters, we established a total of seven test groups, each consisting of varying proportions of failed cutters and different depths of partial wear. The detailed parameters for each test group are provided in Table 4. In practical engineering, it has been observed that disc cutters installed farther away from the center of the cutterhead experience a higher probability of failure (Li, 2021). Thus, the arrangement of failed cutters was from the outer periphery to the inner ring of the cutterhead, with an increasing proportion of failures. Each test group was repeated three times, with an excavation distance of 10 mm per repetition. The average values were calculated and reported as the final results of this paper.

2.3 Experimental Results and Analysis

Excavation parameters have been widely adopted in various models to investigate the interaction mechanisms between disc cutters and rock (Yang et al., 2021). Among them, the thrust along the tunnel axis and the cutterhead torque around it are considered to represent the excavation load of a cutter group and are regarded as key indicators for measuring the tunneling efficiency of a shield. The former represents the cumulative sum of the normal forces applied to all disc cutters, while the latter corresponds to the cumulative sum of the product of the rolling forces acting on the disc cutters and their respective installation radii. Consequently, the variations in these two parameters reflect the changes in the cutting forces of the disc cutters, serving as indicators of disc-cutter health status.

Fig. 7 illustrates the torque and thrust curves for different types of disc cutters. It can be seen that during the initial stage of shield tunneling, these two parameters rapidly increased and tended to stabilize, while exhibiting periodic fluctuations. This phenomenon is consistent with the experimental observations of disc-cutter pressure distribution conducted by Rostami (Rostami, 2013) and the simulation results based on the discrete/finite-element models by Labra (Labra et al., 2017). Additionally, She's research (She et al., 2022) has confirmed the contribution of dense core to the variations in cutting forces during rock-cutting processes. These findings indicate that the rapid increase in cutting forces is primarily attributable to the elastic-plastic deformation experienced by the disc cutter upon initial contact with the rock. As the rock approaches its strength limit, it begins to fracture, resulting in a sharp decrease in cutting forces. Consequently, the rock-breaking load exhibits a periodic fluctuation pattern during excavation. When normal cutters become trapped and unable to rotate, the torque and thrust experience significant increase (1#, 2#, 4#, 6#), leading to a substantial decrease in the rock-breaking efficiency of the cutters. With regard to the cutter's rock-breaking mechanism, the change in motion pattern increases the sliding friction force, which is much greater than the rolling friction force, thereby significantly increasing the rolling forces exerted by the cutters and resulting in increased torque. The alteration in the geometric shape of the cutter's contact area influences the rock-fragmentation mode, causing accumulation of rock powder in the plane (contact region II in the Fig. 6) and consequently increasing the normal force, which leads to an increase in thrust. When the contact areas on the trapped cutters begin to develop wear, the length of the plane increases with the depth of partial wear, further enlarging the sliding friction between the cutters and the rock and resulting in slight increases in thrust and torque (2# and 3#-1, 4# and 5#-1, 6# and 7#-1). However, compared to the failure of normal cutters, these changes are relatively minor.

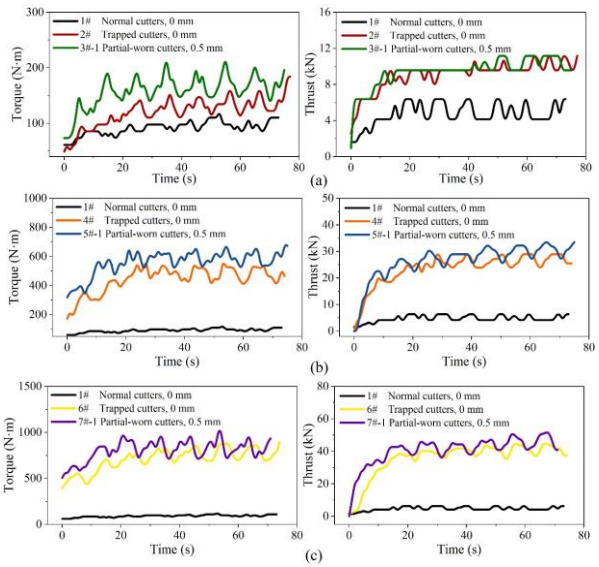

Fig. 7 Torque and thrust of different proportions of failed cutters: (a) 25%, (b) 50%, (c) 75%.

Fig. 8 presents the average values and standard deviations of torque and thrust obtained for each test

group (see Fig. 7), which are statistical features of the data signals in the time domain. The torque and thrust were smallest in all cases where the cutters were in normal condition. The standard deviations were also the smallest for normal cutters, indicating relatively low fluctuation, with a small difference between the maximum and minimum cutting forces (1#). This could be attributed to the intact circular contact area, which maintained relatively stable contact with the rock. As the number of partially worn cutters increased, indicating a higher failure ratio (25%, 50%, 75%), noticeable increases in torque and thrust, along with larger standard deviations, were observed (1#, 2#, 4#, 6#). However, the impact of partial wear (with the same partial-wear ratio) on the standard deviation was found to be insignificant, and in some cases, it even led to a reduction in the standard deviation (4# and 5#-1, 6 and 7#-1). This suggests that enlarging the plane area does not significantly affect contact stability between the cutters and the rock, and has only a minor influence on the extent of load fluctuation.

The torque and thrust at different partial-wear depths are compared in Fig. 9, providing a more intuitive demonstration of the significant impact of partial-wear ratio on shield-tunneling parameters. When the ratio was 25% (2#, 3#-1, 3#-2, 3#-3, 3#-4), both the mean and standard deviation of torque and thrust showed an increasing trend. This is most likely due to the enlarged partial-wear contact area resulting in an increase in the normal forces and sliding friction forces on the cutters. When the partial-wear ratio reached 50% (4#, 5#-1, 5#-2, 5#-3, 5#-4), the rate of increase in the mean values became slower, and the standard deviation tended to stabilize. Finally, when the partial-wear ratio reached 75% (6#, 7#-1, 7#-2, 7#-3, 7#-4), fluctuations in torque and thrust were observed at a partial-wear depth of 1mm. This is probably due to the extreme level of cutter failure, in which the rock-breaking capacity of the shield had reached its limit. At this stage, the front face of the cutterhead was covered by soil and rock, and the advancement of excavation heavily depended on the scrapers and edge cutters positioned along the outer edge of the cutterhead.

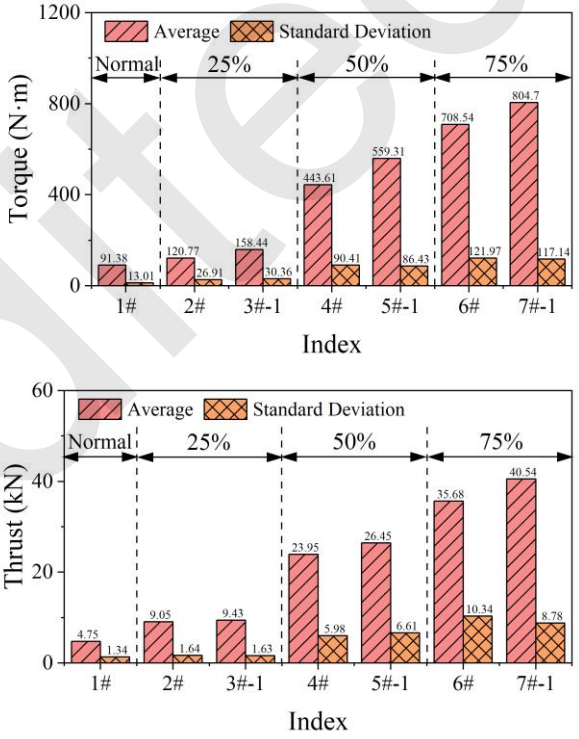

Fig. 8 Torque and thrust statistics

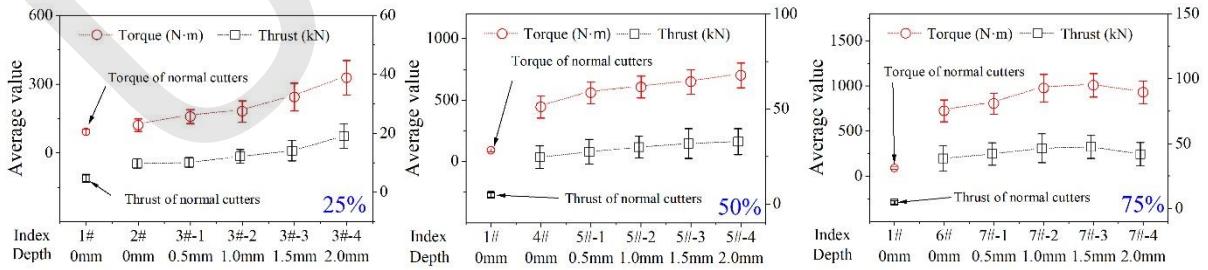

Fig. 9 Average torque and thrust with different partial-wear depth

3. Partial-Wear-Ratio Discrimination Method and Validation

Based on the experimental results analyzed in Section 2.3, we concluded that the partial-wear ratio of disc cutters (i.e., the number of partially worn cutters) has a much greater impact than the degree of wear on tunneling parameters and rock-breaking per-

formance in shield tunneling . The analysis in this section not only focuses on the mean and standard deviation but also extracts additional features from the time domain, frequency domain, and time-frequency domain to reveal their correlations with the partial-wear ratio. Furthermore, we propose and validate an ensemble-learning-based model for partial-wear-ratio discrimination.

3.1 Multi-domain Feature Extraction

Feature extraction is the process of reducing the dimensionality of raw signal data collected by sensors while preserving the essential information embedded within the data (Huang et al., 2022). Time-domain features, such as mean and standard deviation, are used to gain valuable perspectives into temporal characteristics. By transforming the signals from the time domain to the frequency domain using techniques such as Fourier transform, frequency-domain analysis reveals the underlying frequency content and periodic patterns within the data. Furthermore, integration of time and frequency domains in time-frequency-domain analysis provides understanding of the temporal and spectral characteristics of the torque and thrust signals.

(1) Time domain

The specific features of the time domain include mean, standard deviation, root mean square, square root amplitude, peak-to-peak, skewness, kurtosis, form factor, crest factor, impulse factor, clearance factor, and energy. These features are calculated using their respective formulas (Liu et al., 2021; Qin et al., 2023), which are detailed in the Electronic Supplementary Materials.

(2) Frequency domain

The objective of frequency-domain analysis is to identify patterns in the centroid frequency and root mean square frequency changes of the spectrum as the cutter failure rate varies (Yang et al., 2023). The calculation formulas for frequency-domain features are detailed in the Electronic Supplementary Materials.

(3) Time-frequency domain

Time-frequency-domain analysis utilizes wavelet packet decomposition to decompose the raw signal data into multiple sub-bands. The average energy of each sub-band is then extracted as a feature value. This analysis technique addresses limitations of the fixed window of Fourier transform in frequency-domain analysis, and enables direct reflection of non-stationary and short-term features. In this study, we employed the 'db4' wavelet basis function to perform 2-level wavelet packet decomposition on the thrust and torque signal data collected during the tunneling process. This decomposition yielded 4 sub-band signals. The average energy of the wavelet packet coefficients within each sub-band was computed as the feature parameters. This yielded 4 time-frequency-domain features.

In Fig. 10, time-domain waveforms, spectra, and sub-band energies with different partial-wear ratio are presented, using thrust data as an example. The maximum magnitudes of each time-domain waveform were 9.57, 11.17, 30.63, and 45.3. Like the mean and standard deviation discussed in Section 2.3, these magnitudes increased with the rise in partial-wear ratio. As indicated by the calculation formula of time-domain features, the other nine (e.g., RMS, square root amplitude) were correlated with the mean, standard deviation, and maximum values, thus exhibiting certain relationships with the partial-wear ratio. In the frequency domain, there was a gradual decrease in the magnitudes of frequencies with increasing partial-wear ratio, with minimum values of -46.74, -53.56, -58.32, and -62.99. This observation reveals a negative correlation between the minimum frequency magnitudes and partial-wear ratio. Furthermore, based on the calculation formula of frequency-domain features, the four features related to magnitudes, namely the centroid frequency, average frequency, standard deviation of frequency, and root mean square frequency, also convey information about the changes in partial-wear ratio. Wavelet packet decomposition revealed the energy values of the four sub-bands. Over 99% of the energy was concentrated in the first sub-band. In addition, the energy of the first and second sub-bands increased with increasing partial-wear ratio, while the relationship between the energy of the third and fourth sub-bands and the partial-wear ratio was less apparent. Therefore, these four sub-band energy values can serve as preliminary features but will require further investigation into their specific relationships

with partial-wear ratio. To summarize, we focused on torque and thrust signals during excavation. For each type of data, a total of 12 time-domain features, 4 frequency-domain features, and 4 frequency-domain feature selections were extracted, resulting in a total of 40 features. All the features are shown in the Electronic Supplementary Materials.

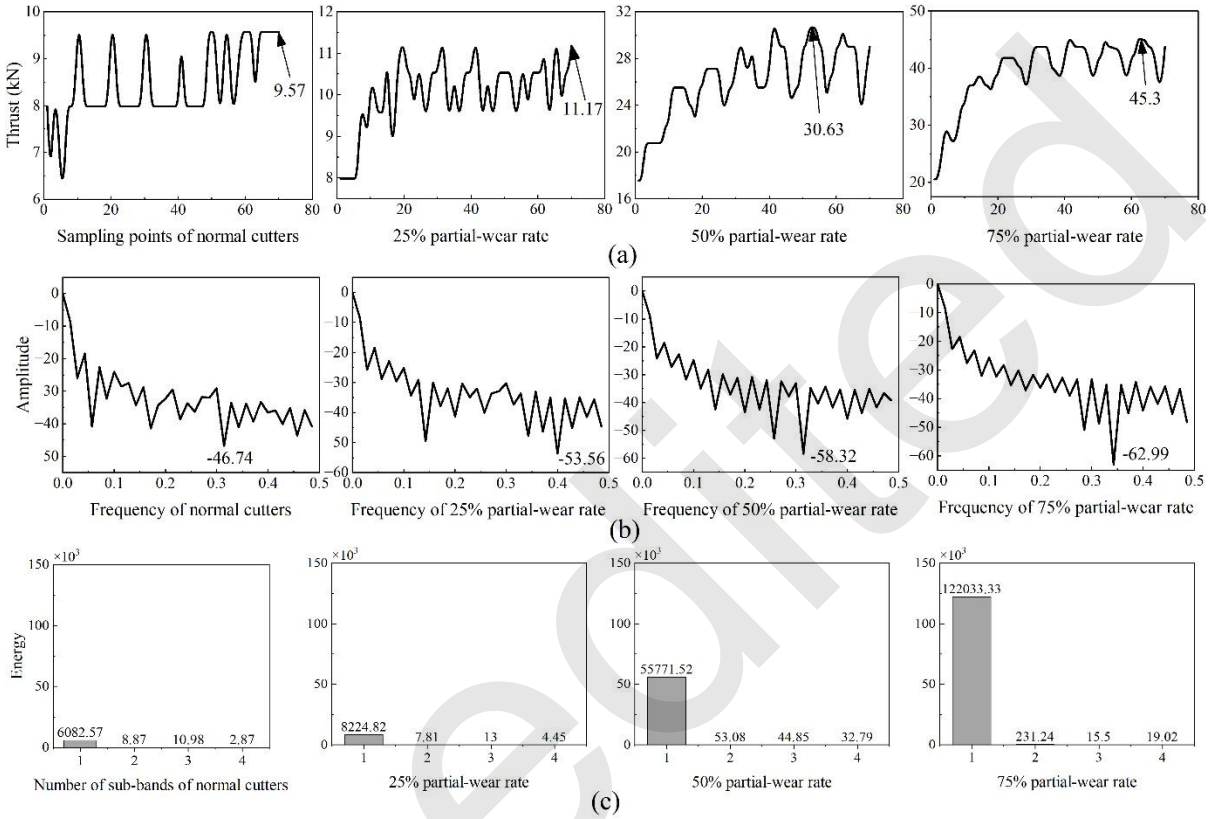

Fig. 10 Multi-domain feature spectrum: (a) Time-domain waveforms, (b) Spectrograms, (c) Sub-band energy diagram

3.2 Feature-Correlation Analysis

In order to investigate the relationship between the features from different domains and partial-wear ratio more comprehensively, we used two correlation analysis methods.

(1) Pearson correlation coefficient

In statistics, the Pearson correlation coefficient (Jiang et al., 2022; Yu et al., 2023) is a widely used measure to quantify the linear relationship between two variables, typically denoted as X and Y. It provides a value between 1 and -1, with a value closer to 1 indicating a stronger positive correlation, a value closer to -1 indicating a stronger negative correlation, and a value close to 0 suggesting a weak (or no linear) correlation. The Pearson correlation coefficient is calculated using the following formula:

$$\rho_{X,Y} = \frac{\operatorname{cov}(X,Y)}{\sqrt{\operatorname{var}(X)\cdot\operatorname{var}(Y)}}. \tag{1}$$

where $\rho(X,Y)$ represents the Pearson correlation coefficient between X and Y; $\operatorname{cov}(X,Y)$ denotes the covariance between X and Y, which measures the joint variability of the two variables; and $\operatorname{var}(X)$ and $\operatorname{var}(Y)$ represent the standard deviations of X and Y, respectively, which quantify the individual variability of each variable.

In Fig. 11, the Pearson correlation coefficients between the 40 extracted features and the partial-wear ratio are presented. The absolute values of these coefficients indicate the strength of the linear relationship. The results demonstrate a strong positive correlation (approximately > 0.5) between the fre-

Uncorrected

quency-domain and time-frequency-domain features and the partial-wear ratio. However, the time-domain features related to thrust and torque, such as skewness, kurtosis, form factor, crest factor, impulse factor, and clearance factor (12 features in total), exhibit no or very weak linear correlation. This implies that these features have limited predictive ability for partial-wear ratio, as their absolute correlation coefficients are less than 0.2 (T_Skewness, T_Kurtosis, T_FormFactor, T_CrestFactor, T_ImpulseFactor, T_ClearanceFactor, F_Kurtosis) or close to 0.2 (F_Skewness, F_FormFactor, F_CrestFactor, F_ImpulseFactor, F_ClearanceFactor). However, considering that these features are commonly used to describe the skewness, sharpness, peak characteristics, and impulse characteristics of data, their weak linear correlation with partial-wear ratio should be interpreted in the context of their primary use for assessing non-linear signal characteristics. Consequently, further exploration of the non-linear relationships between these features and the partial-wear ratio can be pursued using alternative analysis methods.

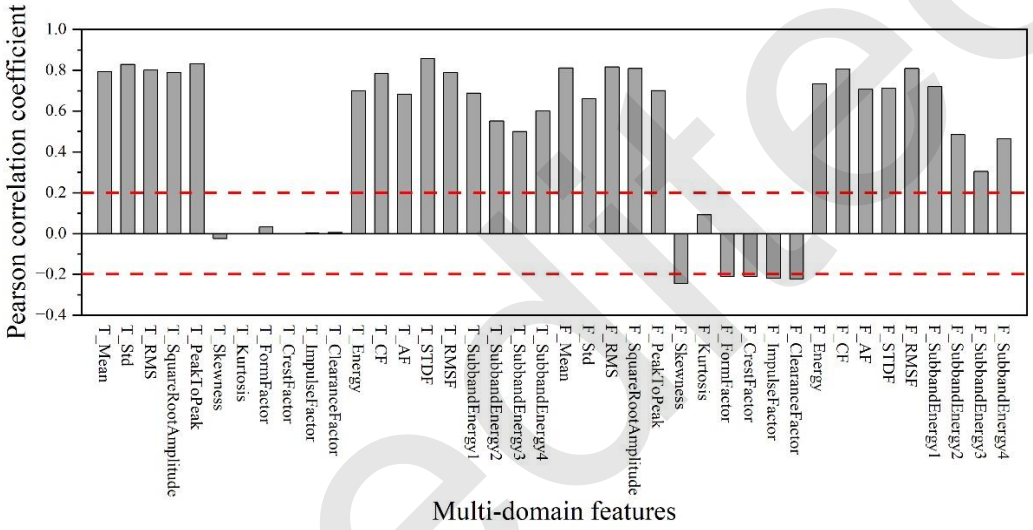

Fig. 11 Pearson correlation coefficients between multi-domain features and partial-wear ratio

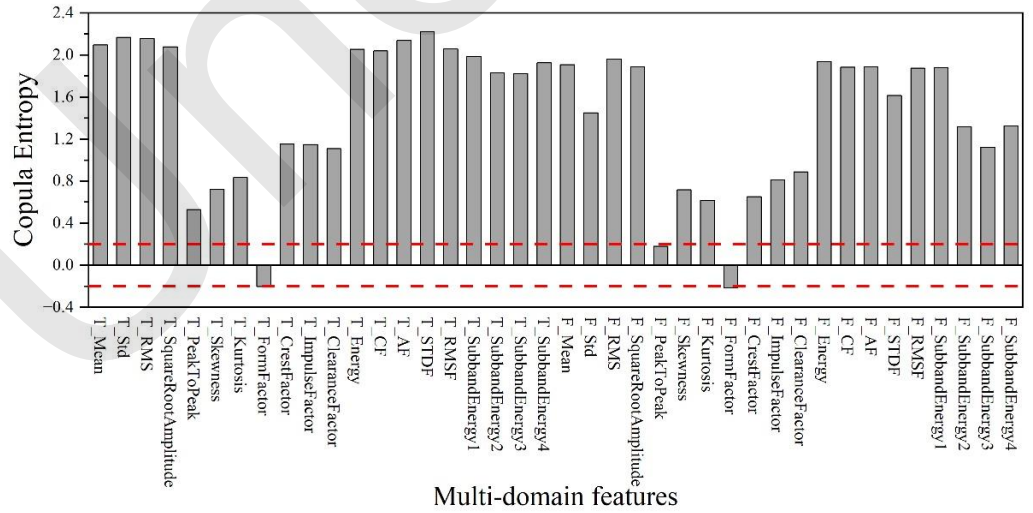

Fig. 12 Copula Entropy between multi-domain features and partial-wear ratio

(2) Copula Entropy

Copula Entropy (CE) can also be utilized as a measure of association between multiple variables (Cui and Sun, 2022). CE quantifies the information content in the relationship and is ideal for assessing

statistical independence. Unlike traditional measures such as Pearson correlation, CE does not rely on model assumptions or complexity, and offers significant advantages in terms of universality. Moreover, entropy is a well-defined concept with clear physical interpretation. CE represents the information content in the functional relationship between the independent variables and the target variable, making it easily comprehensible and interpretable from a physical perspective. Its estimation is based on ordinal statistics, which involves no theoretical assumptions and results in good asymptotic stability and minimal parameter tuning.

Fig. 12 showcases the results of calculating CE between the 40 features and the partial-wear ratio. There is a wealth of information regarding the relationship between partial-wear ratio and the various features in the frequency domain, time-frequency domain, and time domain. The CE values of the 12 features with extremely weak linear correlation, shown in Fig. 12, exhibit noticeable variations. Only the form factor continues to display a remarkably low level of non-linear correlation, while the remaining features demonstrate certain non-linear relationships with the partial-wear ratio. The form factor, which measures the peak characteristics of the signal waveform by comparing the peak value to the effective value, remains unrelated to the partial-wear ratio due to the relatively smooth waveforms and smaller peaks of thrust and torque in this study. Surprisingly, the peak-to-peak value of thrust force (CE = 0.18) shows lower non-linear correlation compared to its linear correlation (Pearson coefficient = 0.70) with the partial-wear ratio. This unexpected finding may be attributable to the less pronounced periodic fluctuations in thrust. After conducting an analysis of both linear and non-linear correlations, we selected a total of 38 features (excluding the form factor) as effective features for discriminating partial-wear ratio.

3.3 Model for Partial-Wear-Ratio Discrimination

(1) Ensemble Learning

Ensemble learning is a powerful machine-learning technique that aims to enhance the predictive accuracy and generalization capability of models by combining multiple weaker base models (Shi et al., 2023; Zhang et al., 2023). It has gained considerable popularity in the field of machine learning due to its ability to improve model performance. There are three common types of ensemble learning models: bagging, boosting, and stacking.

Bagging, short for bootstrap aggregating, involves training multiple base models independently in parallel and then aggregating their predictions using a specific strategy. In classification models, the aggregation can be done through voting, while in regression models, averaging is commonly used. The main idea behind bagging is to reduce variance and increase stability by combining the predictions of diverse base models.

Boosting, on the other hand, is a sequential ensemble learning method in which multiple base models of the same type are trained in sequence (Wang et al., 2022). Each subsequent model is trained to correct the prediction mistakes made by previous models. By focusing on instances that were incorrectly predicted, boosting aims to improve the overall performance of the ensemble model.

Stacking is a more complex ensemble learning technique that involves training multiple base models independently in parallel and then training a meta-model to combine their outputs (Hou et al., 2022). Unlike bagging and boosting, stacking allows for the use of different algorithms to train the base models. The training process of a stacking model typically involves splitting the training dataset into K folds, training different base models' K times, and averaging their training results. The outputs of these base models are then used as input features for the meta-model, which is trained to produce the final prediction.

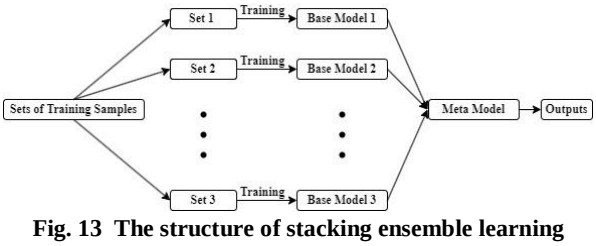

Fig. 13 The structure of stacking ensemble learning

To prevent overfitting, a simple model such as elastic net regression or logistic regression is often used as the meta-model in ensemble learning. The simplicity of the meta-model helps to generalize the

combined predictions of the base models and avoid overfitting to the training data. The structure of stacking ensemble learning is shown in Fig. 13. Overall, ensemble learning leverages the strengths of multiple models and mitigates the weaknesses each individual model, resulting in improved prediction accuracy and generalization.

(2) Partial-Wear-Ratio Discrimination Model (PRDM)

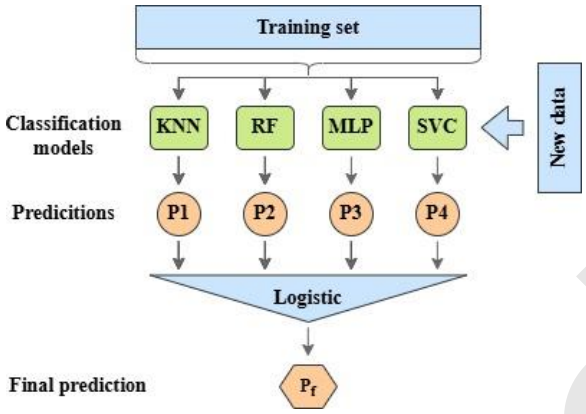

Fig. 14 The specific structure of the PRDM

In this paper, we propose a novel model for predicting the partial-wear ratio of disc cutters, which combines the predictions of multiple base models using stacking ensemble learning. The base models employed in the stacking model include K-Nearest Neighbor (KNN), Random Forest (RF), Support Vector Machine (SVC), and Multilayer Perceptron (MLP). These models are trained independently and their outputs are used as input features for the meta-model, which is a logistic regression (LR) model. The specific structure of the model is illustrated in Fig. 14.

The ensemble learning model utilizes a feature space consisting of the 38 features discussed in Section 3.2, which serve as input features for the model's dataset. The model's output comprises various partial-wear ratio, including the normal state (1#) as well as ratio of 25% (2#), 50% (4#), and 75% (6#). These states are encoded as 0, 1, 2, and 3, respectively, representing the output categories of the model. To ensure optimal model performance and mitigate issues such as overfitting or underfitting, appropriate hyperparameters must be carefully selected. However, manual hyperparameter selection can be time-consuming and prone to error. To address this, we employed the grid search method, systematically exploring different combinations of hyperparameters and evaluating each combination through cross-validation. In addition, we selected commonly used accuracy evaluation metrics for the models , which represent the ratio of correctly categorized samples to the total number of samples, as shown in Eq. (2).

$$Accuracy = \frac{\text{Number of correctly categorized samples}}{\text{Total number of samples}}. \quad (2)$$

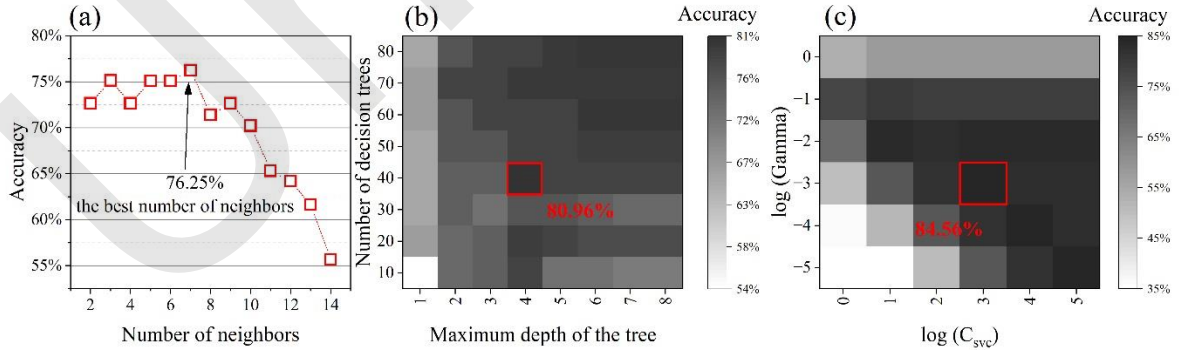

Fig. 15 Grid-search results for the models: (a) KNN, (b) RF, (c) SVC

Fig. 15 illustrates the grid-search results for the three base models: KNN, RF, and SVC. For the KNN model, the highest classification accuracy (76.25%) is achieved when the number of neighbors (n_neighbors) is set to 7. In the RF model, optimal performance is obtained by setting the number of decision trees (n_estimators) to 40 and the maximum depth of each tree (max_depth) to 4, resulting in an accuracy of 80.96%. For the SVC model, the best result is obtained by adjusting the penalty parameter

(C_{svc}) and the width parameter (gamma) of the Gaussian kernel. Specifically, a penalty parameter of 1000 and a width parameter of 0.001 yield the optimal outcome (84.56%).

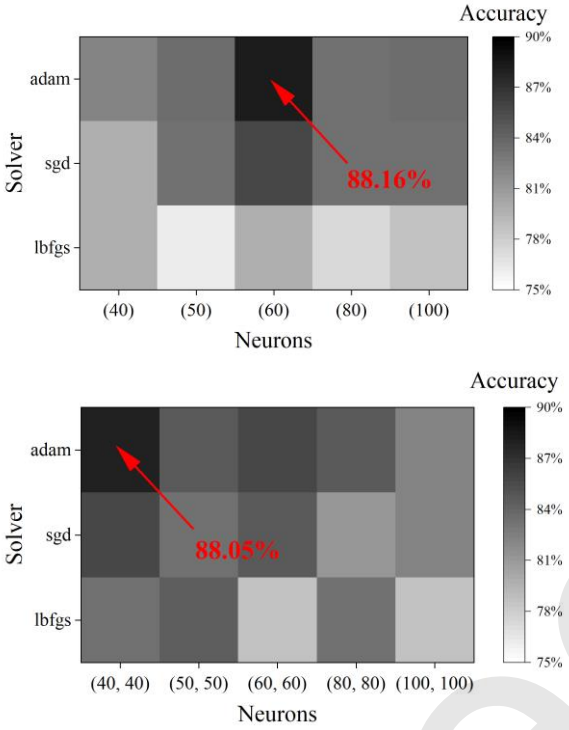

Fig. 16 Grid-search results for the MLP model

The grid-search results for the MLP model with single-layer and two-layer hidden configurations are presented in Fig. 16. In the case of a single-layer hidden configuration, an accuracy of 88.16% was achieved when the neuron size was set to (60) and the solver was selected as Adam. For a two-layer hidden configuration with neuron sizes set to (40, 40) and using the Adam solver, the accuracy slightly decreased to 88.05%, a bit lower than that of the single-layer hidden configuration.

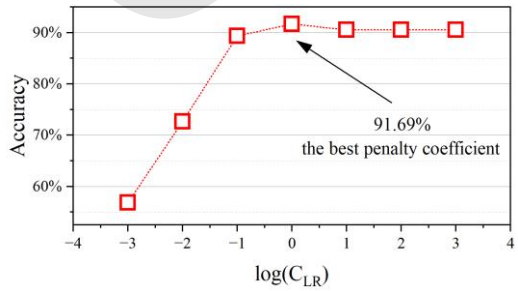

Fig. 17 Results for the LR model

In Fig. 17, it can be observed that the meta-model LR achieved the best discriminative performance when the penalty coefficient (CLR) iwass set to 1.0. In summary, the selected model hyperparameters are shown in Table 5.

Table 5 Set values of model hyperparameters

Models	Hyperparameters	Set values
KNN	n_neighbors	7
RF	n_estimators, max_depth	40, 4
SVC	C_{svc}, gamma	1000, 0.001
ML	Solver, hidden_layer_size	Adam, (60)
LR	C_{LR}	1.0

3.4 Results and Evaluation

In Section 3.3, we described how the accuracy evaluation metric of was used for hyperparameter tuning, which focuses on the overall classification accuracy of the model without considering the differences between categories. To account for the performance of each individual category, we introduced the macro-F1 metric, which combines precision and recall for each category. The macro-F1 calculates the F1 score for each category and then averages their performance to obtain a comprehensive performance measure. The calculation formula is as follows (Eq. (3)).

$$\begin{aligned}\text{macro-P} &= \frac{1}{n}\sum_{i=1}^{n} P_i,\\ \text{macro-R} &= \frac{1}{n}\sum_{i=1}^{n} R_i,\\ \text{macro-F1} &= \frac{2\times\text{macro-P}\times\text{macro-R}}{\text{macro-P}+\text{macro-R}}.\end{aligned} \tag{3}$$

where P_i denotes the precision rate for each category, R_i is the recall rate for each category, and macro-P and macro-R represent the average precision and recall across all categories, respectively.

Uncorrected

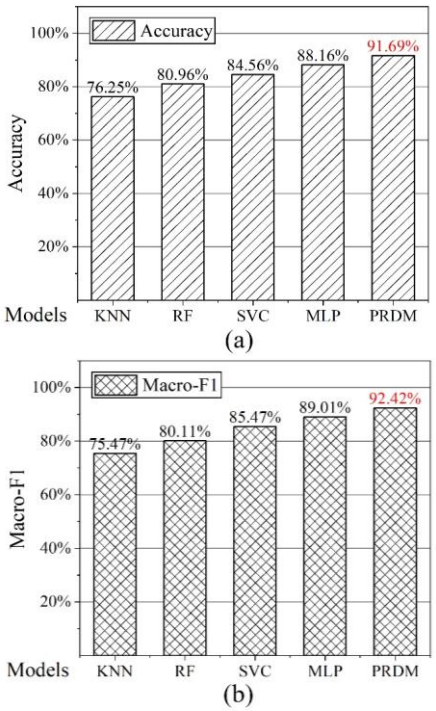

Fig. 18 Comparison results of the models: (a) Accuracy, (b) Macro-F1

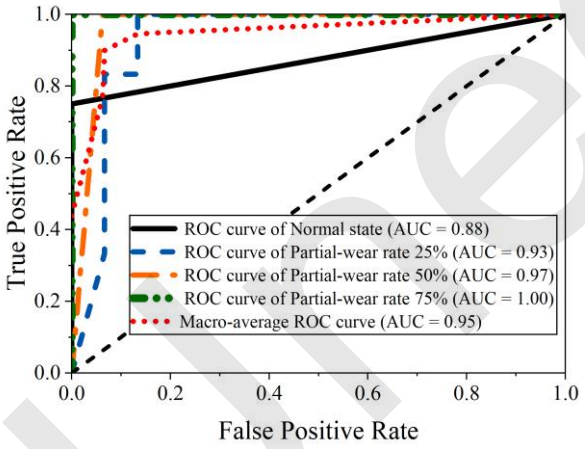

Fig. 19 ROC curves of PRDM

The results of the model comparison are presented in Fig. 18. It can be observed that PRDM achieved the highest values for both accuracy, which emphasizes classification accuracy, and macro-F1, which focuses on the overall performance and balance across multiple classes, with values of 91.69% and 92.42%, respectively. This indicates that the PRDM model can accurately discriminate partial-wear ratio. Additionally, to investigate the model's classification performance for each partial-wear ratio, we plotted Receiver Operating Characteristic (ROC) curves for each category and calculated the average area under the ROC curve (AUC) for each category, as shown in Fig. 19. As the partial-wear ratio increases, the model's discrimination performance improves, even reaching 100% accuracy at a partial-wear ratio of 75%. This further demonstrates that as the partial-wear ratio increases, the changes in torque and thrust become more pronounced, making their associated features more prominent. Furthermore, we calculated the macro-average ROC, which focuses on the model's ability to differentiate and accurately classify different classes, and it also achieved 95%.

In conclusion, evaluation and comparative analysis revealed the outstanding discriminatory performance of the PRDM model, which is built on multi-domain features and stacking ensemble learning. This demonstrates its value as a tool for detection and early warning of disc-cutter failure in TBM operations.

4. Conclusions

In this study, we conducted a series of shield-tunneling experiments on normal disc cutters and disc cutters with a certain proportion of partial wear and different partial-wear depth, aiming to investigate the variation in tunneling parameters and propose an accurate method for discriminating disc-cutter partial-wear ratio. Based on the experimental results, we can draw the following key conclusions:

(1) When abnormal damage occurs to normal disc cutters in the cutterhead, the torque and thrust in tunneling parameters increase. This is attributed to the change in the motion mode between the disc cutters and the rock (from rolling to sliding) and the alteration of the geometric profile of the disc-cutter rings.

(2) The increase in partial-wear ratio, i.e., the increase in the number of partially worn cutters, has a much greater impact on tunneling parameters compared to partial-wear depth. With higher partial-wear ratio, the mean values of torque and thrust significantly increase. In contrast, at the same partial-wear ratio, the increase in partial-wear depth causes only a small change in the magnitude of the mean values of torque and thrust. This may be because the change in the motion mode has a higher impact than the alteration in the geometric profile.

Unedited

(3) Partial-wear depth has a relatively small influence on the cyclic fluctuation of torque and thrust. Standard deviations may even decrease with an increase in partial-wear depth, given the same partial-wear ratio. This is because the enlargement of the contact area between the partial-wear disc cutter and the rock does not affect the stability of the contact.

(4) There is a certain degree of correlation between time-domain, frequency-domain, and time-frequency-domain features and the partial-wear ratio. The magnitude of Pearson correlation coefficients indicates linear correlations between 28 features such as RMS, CF, and sub-band energy and the partial-wear ratio, while the magnitude of CE confirms nonlinear correlations between 12 features such as skewness and kurtosis and the partial-wear ratio.

(5) The proposed PFDM model can accurately discriminate partial-wear ratio. Compared to models such as KNN, RF, SVC, and MLP, PRDM performs the best in terms of accuracy and macro-F1 evaluation metrics. Analysis of ROC curves also demonstrates that the model exhibits good discrimination and judgment accuracy on different partial-wear ratio.

Future work will focus on investigating the impact of partial wear on tunneling parameters under different geological conditions. Additionally, we hope to explore the application of the proposed model in engineering projects in further studies.

Acknowledgments

This work is supported by the Natural Science Basic Research Program of Shaanxi Province (No. 2019JLZ-13), the National Key R&D Program of China (No. 2022YFC3802305), the National Natural Science Foundation of China (No. 52105074), and the Open Project of State Key Laboratory of Shield Machine and Boring Technology (No. SKLST-2021-K02).

Author contributions

Xinghai ZHOU designed the research. Yakun ZHANG processed the corresponding data. Xinghai ZHOU wrote the first draft of the manuscript. Guofang GONG and Huayong YANG helped to organize the manuscript. Xinghai ZHOU revised and edited the final version.

Conflict of interest

Xinghai ZHOU, Yakun ZHANG, Guofang GONG, Huayong YANG declare that they have no conflict of interest.

Reference

Acaroglu O, Ozdemir L, Asbury B, 2008. A fuzzy logic model to predict specific energy requirement for TBM performance prediction. *Tunnelling and Underground Space Technology*, 23(5):600-608. https://doi.org/10.1016/j.tust.2007.11.003

Amoun S, Sharifzadeh M, Shahriar K, et al., 2017. Evaluation of tool wear in EPB tunneling of Tehran Metro, Line 7 Expansion. *Tunnelling and Underground Space Technology*, (61):233-246. https://doi.org/10.1016/j.tust.2016.11.001

Bilgin N, Algan M, 2012. The performance of a TBM in a squeezing ground at Uluabat, Turkey. *Tunnelling and Underground Space Technology*, 32:58-65. https://doi.org/10.1016/j.tust.2012.05.004

Cui S, Sun S, 2022. Study on the correlation of wind turbine variables under different conditions. *Integrated Intelligent Energy*, 12(44):51-55. https://doi.org/10. 3969/j. issn. 2097-0706. 2022. 12. 007

Farrokh E, Rostami J, 2008. Correlation of tunnel convergence with TBM operational parameters and chip size in the Ghomroud tunnel, Iran. *Tunnelling and Underground Space Technology*, 23(6):700-710. https://doi.org/10.1016/j.tust.2008.01.005

Hassanpour J, 2018. Development of an empirical model to estimate disc cutter wear for sedimentary and low to medium grade metamorphic rocks. *Tunnelling and Underground Space Technology*, (75):90-99. https://doi.org/10.1016/j.tust.2018.02.009

Hassanpour J, Rostami J, Tarigh Azali S, et al., 2014. Introduction of an empirical TBM cutter wear prediction model for pyroclastic and mafic igneous rocks; a case history of Karaj water conveyance tunnel, Iran. *Tunnelling and Underground Space Technology*, (43):222-231. https://doi.org/10.1016/j.tust.2014.05.007

Hou S, Liu Y, Yang Q, 2022. Real-time prediction of rock mass classification based on TBM operation big data and stacking technique of ensemble learning. *Journal of Rock Mechanics and Geotechnical Engineering*, 14(1):123-143. https://doi.org/10.1016/j.jrmge.2021.05.004

Huang H, Yao J, Xue W, et al., 2022. Tool wear state recognition based on joint distribution adaptation of multi-domain feature. *Computer Integrated Manufacturing Systems*, 28(08):2419-2429. https://doi.org/10.13196/j.cims.2022.08.013

Huang J, 2021. Application and Research of Composite Shield Disc Cutter in Quartzite Stratum Excavation. *Construction Technology*, 50(11):124-128. https://doi.org/10.7672/sgjs2021110124

Jiang Y, Liu Q, Zhu B, et al., 2022. Correlation Analysis of Machine Performance Parameters and Rock Mass Properties during Tunnel Boring Machine Excavation Process: A Case Study in Yin-song Headrace Tunnel, China. *Journal of Testing and Evaluation*, 50(6):2883-2900. https://doi.org/10.1520/JTE20200639

Karami M, Zare S, Rostami J, 2021. Tracking of disc cutter

Unedited

wear in TBM tunneling: a case study of Kerman water conveyance tunnel. *Bulletin of Engineering Geology and the Environment*, 80(1):201-219. https://doi.org/10.1007/s10064-020-01931-7

Ko TY, Lee SS, 2020. Effect of Rock Abrasiveness on Wear of Shield Tunnelling in Bukit Timah Granite. *Applied Sciences-Basel*, 10(9):15. https://doi.org/10.3390/app10093231

Labra C, Rojek J, Onate E, 2017. Discrete / Finite Element Modelling of Rock Cutting with a TBM Disc Cutter. *Rock Mechanics and Rock Engineering*, 50(3):621-638. https://doi.org/10.1007/s00603-016-1133-7

Lan H, Xia Y, Ji Z, et al., 2019. Online monitoring device of disc cutter wear - Design and field test. *Tunnelling and Underground Space Technology incorporating Trenchless Technology Research*, (89):284-294. https://doi.org/10.1016/j.tust.2019.04.010

Li J, Nie Y, Fu K, et al., 2018. Experiment and analysis of the rock breaking characteristics of disc cutter ring with small edge angle in high abrasive grounds. *Journal of The Brazilian Society of Mechanical and Engineering*, 40(10):12. https://doi.org/10.1007/s40430-018-1422-z

Li X, Su X, 2010. A new method for forecasting shield's disc-cutters wearing based on Elman neural network. *Journal of Liaoning Technical University (Natural Science)*, 29(06):1121-1124. https://doi.org/10.3969/j.issn.1008-0562.2010.06.030

Li Y, 2021. Failure Form and Cause Analysis of EPB Shield Cutter in a Water Diversion Project in Xinjiang. *Modern Manufacturing Technology and Equipment*, 57(9):51-54. https://doi.org/10.16107/j.cnki.mmte.2021.0712

Lin L, Xia Y, Zhang X, 2020. Wear Characteristics of TBM Disc Cutter Ring Sliding against Different Types of Rock. *KSCE Journal of Civil Engineering*, 24(10):3145-3155. https://doi.org/10.1007/s12205-020-2208-2

Liu B, Yang H, Karekal S, 2021. Reliability analysis of TBM disc cutters under different conditions. *UNDERGROUND SPACE*, 6(2):142-152. https://doi.org/10.1016/j.undsp.2020.01.001

Liu Z, Wang B, Shang W, 2017. Study of Wireless Detection System of Shield Cutter Wear Based on Ultrasonic. *Tunnel Construction*, 11(37):1469-1474. https://doi.org/10.3973/j.issn.2096-4498.2017.11.017

Pan Y, Liu Q, Liu Q, et al., 2020. Full-scale linear cutting tests to check and modify a widely used semi-theoretical model for disc cutter cutting force prediction. *Acta Geotechnica*, 15(6):1481-1500. https://doi.org/10.1007/s11440-019-00852-4

Qin C, Wu R, Huang G, et al., 2023. A novel LSTM-autoencoder and enhanced transformer-based detection method for shield machine cutterhead clogging. *Science China-Technological Sciences*, 66(2):512-527. https://doi.org/10.1007/s11431-022-2218-9

Ren D, Shen S, Arulrajah A, et al., 2018. Prediction Model of TBM Disc Cutter Wear During Tunnelling in Heterogeneous Ground. *Rock Mechanics and Rock Engineering*, 51(11):3599-3611. https://doi.org/10.1007/s00603-018-1549-3

Rostami J, 2013. Study of pressure distribution within the crushed zone in the contact area between rock and disc cutters. *International Journal of Rock Mechanics and Mining Sciences*, 57:172-186. https://doi.org/10.1016/j.ijrmms.2012.07.031

She L, Zhang S, Wang C, et al., 2022. A cutting mechanics model of constant cross-section type disc cutter and its application based on dense core theory. *International Journal of Rock Mechanics and Mining Sciences*, 150. https://doi.org/10.1016/j.ijrmms.2021.105025

Shi M, Hu W, Li M, et al., 2023. Ensemble regression based on polynomial regression-based decision tree and its application in the in-situ data of tunnel boring machine. *Mechanical Systems and Signal Processing*, 188. https://doi.org/10.1016/j.ymssp.2022.110022

Su W, Li X, Jin D, et al., 2020. Analysis and prediction of TBM disc cutter wear when tunneling in hard rock strata: A case study of a metro tunnel excavation in Shenzhen, China. *Wear*, 446:11. https://doi.org/10.1016/j.wear.2020.203190

Sun R, Mo J, Zhang M, et al., 2022. Cutting performance and contact behavior of partial-wear TBM disc cutters: A laboratory scale investigation. *Engineering Failure Analysis*, 137:15. https://doi.org/10.1016/j.engfailanal.2022.106253

Sun R, Mo J, Zhang M, et al., 2023. Interaction between partial-worn TBM cutters and rocks: experimental and numerical investigation. *Bulletin of Engineering Geology and the Environment*, 82(4):17. https://doi.org/10.1007/s10064-023-03127-1

Wang F, Men C, Kong X, et al., 2019. Optimum Design and Application Research of Eddy Current Sensor for Measurement of TBM Disc Cutter Wear. *Sensors*, 19(19):1. https://doi.org/10.3390/s19194230

Wang Y, Gao X, Jiang P, et al., 2022. An extreme gradient boosting technique to estimate TBM penetration rate and prediction platform. *Bulletin of Engineering Geology and the Environment*, 81(1). https://doi.org/10.1007/s10064-021-02527-5

Yang H, Liu B, Wang Y, et al., 2021. Prediction Model for Normal and Flat Wear of Disc Cutters during TBM Tunneling Process. *International Journal of Geomechanics*, 21(3):10. https://doi.org/10.1061/(ASCE)GM.1943-5622.0001950

Yang J, Qiu C, 2016. Prediction of Cutting Tool Wear Rate. *Construction Technology*, 45(22):25-30. https://doi.org/10.7672/sgjs2016220025

Yang Z, Wang L, Zhou J, et al., 2023. Mechanical characteristics of a tunnel boring machine cutterhead during rock breaking: Physical model tests and transient dynamic analysis. *Advances in Mechanical Engineering*, 15(3). https://doi.org/10.1177/16878132231159971

Yu H, Qin C, Tao J, et al., 2023. A multi-channel decoupled deep neural network for tunnel boring machine torque and thrust prediction. *Tunnelling and Underground Space Technology*, 133. https://doi.org/10.1016/j.tust.2022.104949

Yu H, Tao J, Huang S, et al., 2021. A field parameters-based method for real-time wear estimation of disc cutter on TBM cutterhead. *Automation in Construction*, (124):103603. https://doi.org/10.1016/j.autcon.2021.103603

Yu Q, Long W, Yang X, et al., 2020. Effects of Heat Treatment Process with Different Hardness Gradients on Microstructure and Mechanical Properties of Shield Cutter Ring. *Hot Working Technology*, 12(49):150-152. https://doi.org/10.14158/j. cnki. 1001-3814. 20193719

Zhang GJ, Xiao CY, 2018a. Analysis of thermal stress distribution of TBM disc cutter. *Australian Journal of Mechanical Engineering*, 16:6. https://doi.org/10.1080/1448837X.2018.1545471

Zhang GJ, Xiao CY, 2018b. Analysis of stress distribution of disc cutter under different tunnelling parameters. *Australian Journal of Mechanical Engineering*, 16:49-53. https://doi.org/10.1080/1448837X.2018.1545472

Zhang H, 2011. Mechanical Analysis of TBM Disc Cutter Damage Mechanism and Its Application. *Modern Tunnelling Technology*, 48(1):61-65. https://doi.org/10.13807/j.cnki.mtt.2011.01.018

Zhang N, Shen S, Zhou A, 2023. A new index for cutter life evaluation and ensemble model for prediction of cutter wear. *Tunnelling and Underground Space Technology*, 131. https://doi.org/10.1016/j.tust.2022.104830

Zhang X, Xia Y, Zhang Y, et al., 2017. Experimental study on wear behaviors of TBM disc cutter ring under drying, water and seawater conditions. *Wear*, 392:9. https://doi.org/10.1016/j.wear.2017.09.020

Zhang Y, 2021. Design and Research of Test Platform for Thrust Hydraulic Cylinder in Shield Machine. Master Thesis, China University of Mining and Technology, Xuzhou, China.

Electronic supplementary materials

Sections S1–S4

中文概要

题　目： 圆盘滚刀偏磨对隧道掘进参数的影响研究及其高精度判别

作　者： 周星海，张亚坤，龚国芳，杨华勇

机　构： 浙江大学，流体动力基础件与机电系统全国重点实验室，中国杭州，310058

目　的： 隧道掘进机滚刀失效引起的损耗是工程施工速度和造价的关键因素，滚刀偏磨在异常损坏中最为常见。本文旨在探讨滚刀偏磨故障对掘进参数（刀盘扭矩和推力）的影响，研究偏磨故障率的判别方法，以实现滚刀故障的准确识别。

创新点： 1. 搭建滚刀故障模拟试验台，进行滚刀偏磨故障试验，获取不同偏磨故障率下的掘进参数数据；2. 通过时域、频域及时频域故障特征提取，建立基于 Stacking 集成模型的偏磨故障率判别模型，成功实现滚刀偏磨故障率的高精度判别。

方　法： 1. 通过缩尺偏磨试验，收集不同偏磨状态下刀盘扭矩和推力数据，并对其时域特征进行分析，结果显示滚刀受困并发生偏磨会显著影响刀盘扭矩和推力（图 8-10）；2. 运用时域、频域及时频域分析方法，对偏磨特征进行了精细提取，并采用了 Person 相关系数及 Copula 熵进行特征分析（见图 12-13），最终形成判别模型的数据集；3. 基于 Stacking 集成模型算法，建立偏磨故障率判别模型，并与 KNN、RF、SVC、ML 等经典模型进行全面对比，验证所提模型的有效性和准确性（图 19-20）。

结　论： 1. 当盾构滚刀受困并出现偏磨时，掘进参数中的推力和扭矩会随之显著增加，这是因为滚刀与岩石的相互运动方式从滑动转变滚动，同时接触区域的形状也发生了变化；2. 相比于偏磨深度，偏磨故障率对掘进参数的影响更为显著；3. 推力和扭矩的多域特征与偏磨故障率之间存在相关性，Pearson 相关系数的大小表明了 RMS、CF 和子带能量等 28 个特征与偏磨故障率之间的线性相关性，而 CE 则确认了偏度和峰度等 12 个特征与偏磨故障率之间的非线性相关性；4. 所提出的 PFDM 模型能够准确判别偏磨故障率，与 KNN、RF、SVC 和 MLP 等模型相比，PRDM 在准确性和宏观 F1 评估指标方面表现最佳。

关键词： 隧道掘进机；滚刀；偏磨；掘进参数；多域特征；集成学习

Under